

SPECIAL
ISSUE

Towards Catalytic Antibiotics: Redesign of Aminoglycosides To Catalytically Disable Bacterial Ribosomes

Boris Smolkin,^[a] Alina Khononov,^[a] Tomasz Pieńko,^[b, c] Michal Shavit,^[a] Valery Belakhov,^[a] Joanna Trylska,^[b] and Timor Baasov^{*[a]}

The emergence of multidrug-resistant pathogens that are resistant to the majority of currently available antibiotics is a significant clinical problem. The development of new antibacterial agents and novel approaches is therefore extremely important. We set out to explore the potential of catalytic antibiotics as a new paradigm in antibiotics research. Herein, we describe our pilot study on the design, synthesis, and biological testing of a series of new derivatives of the natural aminoglycoside antibiotic neomycin B for their potential action as catalytic antibiotics. The new derivatives showed significant antibacterial activity against wild-type bacteria and were especially potent

against resistant and pathogenic strains including *Pseudomonas aeruginosa* and methicillin-resistant *Staphylococcus aureus*. Selected compounds displayed RNase activity even though the activity was not as high and specific as we would have expected. On the basis of the observed chemical and biochemical data, along with the comparative molecular dynamics simulations of the prokaryotic rRNA decoding site, we postulate that the rational design of catalytic antibiotics should involve not only their structure but also a comprehensive analysis of the rRNA A-site dynamics.

Introduction

The ongoing emergence of multidrug-resistant pathogens requires continuous intensive search for novel antibiotics. Unfortunately, only two new classes of antibiotics, oxazolidinones^[1] and lipopeptides,^[2] have been introduced into clinical practice during the last decades. Furthermore, it is well documented that once a new antibiotic is introduced into the clinic, whether it is a novel chemical entity acting at a distinct bacterial target or a semisynthetic derivative that counters the resistance to its parent drug, within only a short matter of time new resistance will emerge and create a serious public health problem.^[3] Some bacterial strains have developed multidrug resistance that covers the majority of currently available antibiotics. The significance of this health problem has re-ener-

gized the search for new antibacterial agents and novel approaches.

One innovative approach is the development of catalytic antibiotics: the pharmacophore of an existing antibiotic is modified to include a catalytic warhead that disables the target in a catalytic manner. Unlike conventional antibiotics that act on their targets in either a reversible (noncovalent interaction) or an irreversible manner (covalent interaction), the antibiotics acting in a catalytic manner promote multiple turnovers of a catalytic cycle. The possible benefits include 1) activity at lower dosages and consequently reduced side effects, 2) activity against drug-resistant bacteria, and 3) reduced potential for generating new resistance.


In general, the idea of catalytic drugs is not novel and several studies towards the development of such agents have been reported previously.^[4,5] These include numerous peptide-cleaving agents based on small-molecule metal complexes as artificial proteases,^[4] site-specific RNA-cleaving agents that combine a reactive moiety (phosphodiester cleavage directed, nonmetallic warhead) with a recognition element (sequence-specific hybridization to target RNA),^[6] and nonmetallic small-organic molecules as artificial ribonucleases.^[7,8]


Inspired by these findings, we set out to explore the potential of catalytic antibiotics as a new paradigm in antibiotics research. Herein, we focus on redesigning aminoglycosides, which represent a particularly well-studied and broad-spectrum class of antibiotics. These molecules exert their therapeutic (bactericidal) effect by selectively binding to the aminoacyl-tRNA binding site (A-site) of the bacterial 16S rRNA, thereby interfering with translational fidelity during protein synthesis.^[9]

[a] Dr. B. Smolkin, A. Khononov, Dr. M. Shavit, Dr. V. Belakhov, Prof. Dr. T. Baasov
The Edith and Joseph Fischer Enzyme Inhibitors Laboratory
Schulich Faculty of Chemistry, Technion—Israel Institute of Technology
Haifa 3200003 (Israel)
E-mail: chtimor@technion.ac.il

[b] Dr. T. Pieńko, Prof. Dr. J. Trylska
Centre of New Technologies, University of Warsaw
Banacha 2c, 02-097 Warsaw (Poland)

[c] Dr. T. Pieńko
Department of Drug Chemistry
Faculty of Pharmacy with the Laboratory Medicine Division
Medical University of Warsaw
Banacha 1a, 02-097 Warsaw (Poland)

 Supporting information and the ORCID identification numbers for the authors of this article can be found under <https://doi.org/10.1002/cbic.201800549>.

 This article is part of a Special Issue on the occasion of Chi-Huey Wong's 70th birthday.

Previous reports on the ability of copper–aminoglycoside complexes to promote hydrolytic and oxidative cleavage of RNA^[10–13] have prompted the potential use of these complexes as metallodrugs with potent antibacterial activity. However, antibacterial tests showed no significant enhancement in the activity of the copper–aminoglycoside complex relative to that of the parent aminoglycoside,^[14] this suggests that a more sophisticated design process is needed to obtain a biologically functional catalytic antibiotic.

We hypothesized that by employing the available structural and mechanistic library of data on the aminoglycoside target, natural ribonuclease systems, and recently reported artificial, small-molecule systems capable of cleaving phosphodiester bonds, we could create a new variant of an aminoglycoside antibiotic that would selectively and catalytically act on the bacterial ribosome and irreversibly deactivate it. To test this hypothesis, herein we describe our pilot studies on the design, synthesis, and biological evaluation of a series of new neomycin B (NeoB) derivatives (compounds **1–10**, Scheme 1) substituted at the 4'-position (through ether and amide linkages) or at the 6'-position (through an amide linkage) with various diamine moieties as potential catalytic warheads for the hydrolysis of rRNA. The observed data demonstrates that most of the

new derivatives retain the antibacterial potency of the parent NeoB against wild-type strains of both Gram-negative and Gram-positive bacteria and display significantly better activity against the tested resistant strains. Particularly improved activities are observed against methicillin-resistant *Staphylococcus aureus* (MRSA) and *Pseudomonas aeruginosa* strains, both of which are highly resistant to conventional aminoglycosides. Interestingly, three of the 4'-amide derivatives show a twofold stronger inhibition of protein synthesis in comparison to NeoB and other clinically used aminoglycosides. However, all attempts to demonstrate cleavage of the scissile phosphodiester bond of rRNA by these derivatives have been unsuccessful. On the basis of the observed chemical and biochemical data, along with the comparative molecular dynamics simulations of the prokaryotic rRNA decoding site, we postulate that the rational design of the catalytic antibiotics should involve not only their structure but also a comprehensive analysis of the rRNA A-site dynamics.

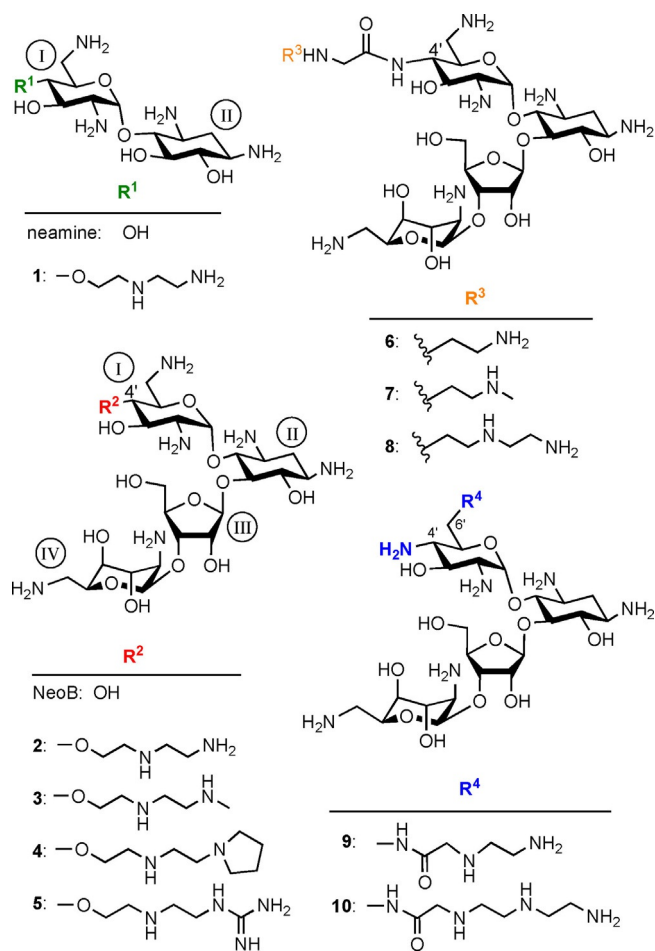
Results and Discussion

Design hypothesis

Initially, we considered the following three key aspects in our design of a potential aminoglycoside catalyst: 1) The choice of the phosphodiester bond in the A-site that should be the most susceptible to catalytic cleavage; 2) the potential “catalytic warhead” structures; 3) the attachment site of a “catalytic warhead” on the aminoglycoside structure.

1) *The choice of the phosphodiester bond:* Compelling evidence is now available that successful cleavage of an RNA phosphodiester bond requires substantial motion in the HO–C2'–C3'–O–P bonds of the ribose-3'-phosphate region to reach the necessary low-energy transition state wherein the C2'–OH group is orientated for in-line nucleophilic attack on the scissile bond.^[7] Such flexibility is usually achieved by enzyme-induced flipping of the base attached to the RNA scissile bond. The mechanisms suggested for RNase T1,^[15] RNase α -sarcin,^[16] and several ribozymes^[17] are only a few of the examples that support this notion. Of particular relevance is the proposed mechanism for colicin E3 (ColE3), a natural enzymatic toxin produced in several *Escherichia coli* strains that selectively cleaves a phosphodiester bond between A1493 and G1494 of 16S rRNA.^[18] This cleavage impairs the protein-translation process and, consequently, leads to cell death. The proposed mechanism of ColE3 also explains why this natural ribonuclease cleaves a specific position in the A-site of rRNA, between A1493 and G1494. This region of the A-site is very important functionally (for correct proofreading) and is also one of the most flexible and accessible regions in the whole ribosome, because it needs to accommodate the incoming aminoacyl-tRNA.

Consequently, we postulated that the target phosphodiester bond must be within the region of rRNA that upon binding of an aminoglycoside undergoes the most extensive conformational change. Moreover, this region is virtually the same as



Scheme 1. Structures of neamine, neomycin B (NeoB), and synthetic aminoglycosides **1–10** that were investigated in this study.

that of ColE3 binding: G1491–A1492–A1493–G1494. Given that the binding of most aminoglycosides induces extensive flipping of the A1492 and A1493 base residues from the bulged-in (ligand-unbound ribosome) to the bulged-out conformation,^[19] similar to that of ColE3 binding,^[20] it is most likely that the best three phosphodiester bond candidates within the A-site are between G1491–A1492, A1492–A1493, and A1493–G1494.

2) The choice of the catalytic warhead: Previous studies with simple diamines demonstrated their ability to accelerate cleavage of adenylyl(3′-5′)-adenosine (ApA) from one to three orders of magnitude more efficiently than the corresponding monoamines.^[21,22] Furthermore, it was shown that the order of reactivity for the simple diamine series was as follows: N-2-N > N-3-N > N-1-N > N-4-N > N-5-N. The strong activities of N-2-N and N-3-N were primarily ascribed to the abundance of catalytically active monocations (61% for N-2-N and 7.4% for N-3-N) that exist at pH 7, because the second protonation is suppressed owing to electrostatic repulsion of the positively charged ammonium ions (the corresponding pK_a values are 6.8 and 9.4 for N-2-N, and 8.1 and 9.8 for N-3-N). On the basis of these observations, we selected ethylenediamine, methyl ethylenediamine, diethylenetriamine, *N*-(2-aminoethyl)pyrrolidine, and guanidine-ethylenamine as potential “catalytic warheads” and prepared new NeoB derivatives **1–10** (Scheme 1).

3) The choice of the attachment site of a catalytic warhead: We selected the 4′-hydroxy group (ring I) of NeoB (Figure 1) as the attachment site for the following reasons. Firstly, the available structural data on the interaction of NeoB with its ribosomal target^[19] indicate that the 4′-hydroxy group is positioned in front of the scissile phosphodiester bond of G1491–A1492 and is near a large cavity formed in the A-site that makes its modification feasible. Secondly, our preliminary molecular modeling studies of the proposed warheads linked at the 4′-position suggested that the phosphodiester bond between G1491 and A1492 was the closest one and that its cleavage was feasible through acid–base catalysis (Figure 1): the terminal amino group in its ammonium form can activate the phosphate be-

tween G1491 and A1492 as a general acid (3.9 Å distance), and the next-nearest amine can activate the 2′-hydroxy group of G1491 as a general base (2.6 Å distance). Finally, Ye and co-workers recently reported a series of new derivatives of kanamycin B modified at the 4′-OH position that showed excellent antibacterial activity against both wild-type and resistant bacteria.^[23] The following findings of this study are of particular importance: 1) the side-chain-free amine is best tolerated by the ribosome; 2) the A-site of the ribosome can accommodate bulky substituents linked at the 4′-position. On the basis of these collective data, we selected the 4′-OH group (ring I) of NeoB as an attachment site for the catalytic warhead and G1491–A1492 as the cleavage site, as schematically illustrated in Figure 1.

Synthesis of 4′-O-linked compounds

To selectively modify NeoB at the desired 4′-position, we initially developed the required synthetic pathway for its simplest fragment, that is, neamine, which consists of rings I and II of NeoB, and prepared derivative **1** as illustrated in Scheme 2. The synthesis started from commercial paromomycin sulfate; it was treated with anhydrous HCl [acetyl chloride (AcCl) in MeOH] at reflux, which resulted in highly regioselective hydrolysis between rings II and III to give paromamine as its hydrochloride salt. The observed salt was converted into the free-base form by passing it through a column of Dowex 50W (H^+ form). Paromamine in its free-base form was then converted into corresponding perazido derivative **11** by a diazo-transfer reaction in the presence of trifluoromethanesulfonyl azide (TfN_3), $CuSO_4 \cdot 5H_2O$, and Et_3N .

Treatment of **11** with benzaldehyde dimethylacetal in dry DMF in the presence of camphorsulfonic acid (CSA) afforded corresponding benzylidene acetal **12**, which was then O-benzylated with benzyl bromide (BnBr) in the presence of NaH in DMF to yield tribenzyl ether **13**. Removal of the benzylidene group (acetic acid, 60 °C) gave corresponding diol **14**, which was then selectively tosylated at the 6′-hydroxy group by using 4-toluenesulfonyl chloride (TsCl) in pyridine (py); this was

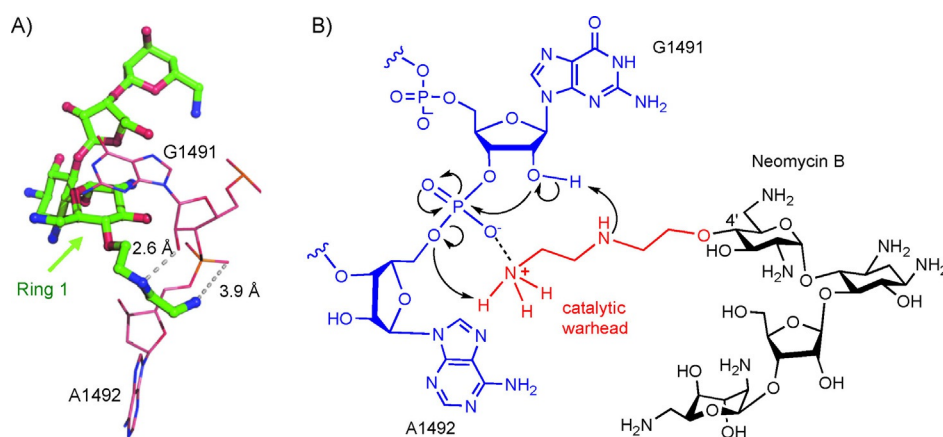
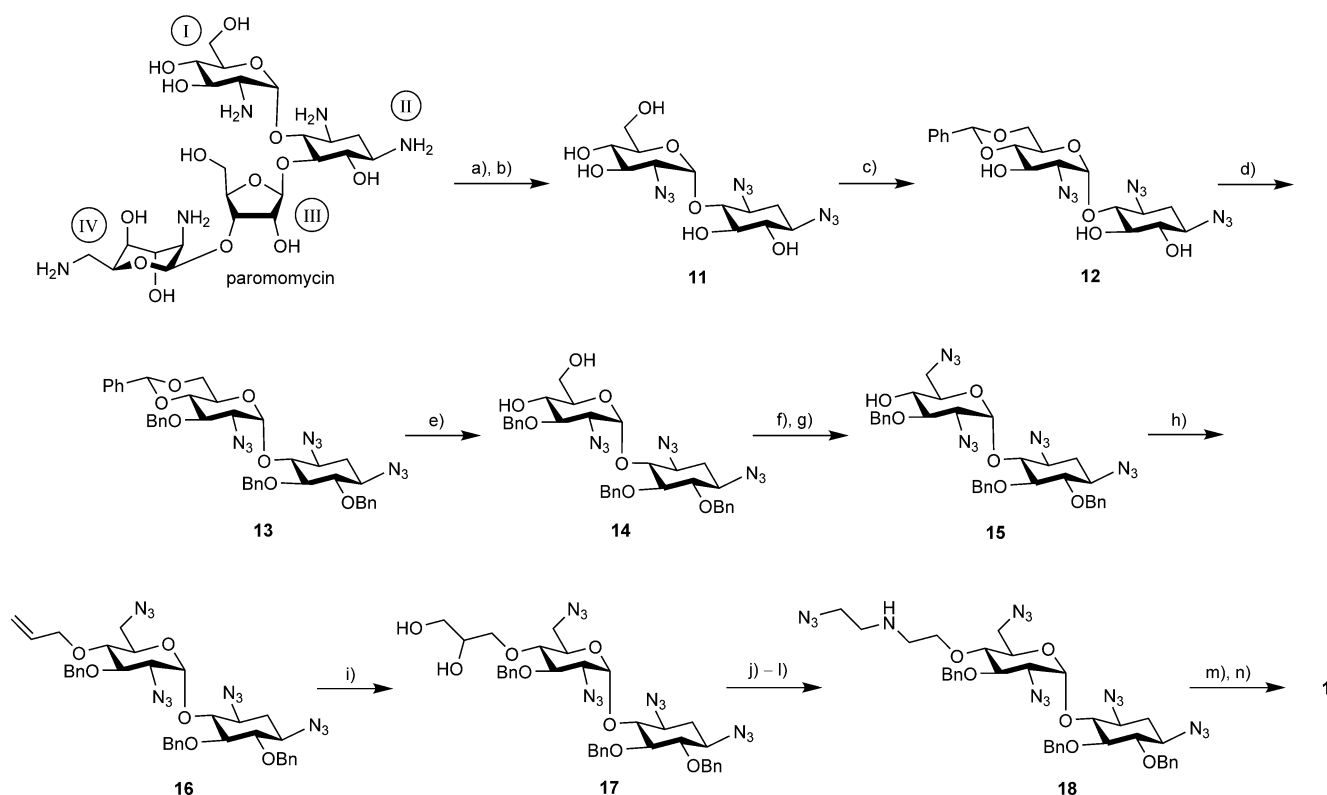


Figure 1. A) Ball-and-stick representation of compound **2**-induced cleavage site in the bacterial rRNA A-site. Modeling was performed by superimposition of **2** with the NeoB structure in the crystal structure of NeoB bound to the rRNA oligonucleotide model (PDB ID: 2ET4)^[19] by using PyMOL. B) Proposed catalytic action of compound **2** on the hydrolysis of the phosphodiester bond between G1491 and A1492.



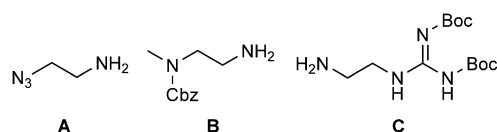
Scheme 2. Chemical transformation of paromomycin into pseudodisaccharide **1**. a) AcCl, MeOH; b) TfN_3 , CuSO_4 (90%); c) PhCH(OMe)_2 , CSA, DMF (83%); d) BnBr, NaH, DMF (88%); e) AcOH/ H_2O (90%); f) TsCl, py; g) NaN_3 , DMF (68%); h) allyl bromide, NaH, DMF (97%); i) K_2OsO_4 , NMO, acetone/ H_2O (80%); j) PhI(OAc)_2 , CH_2Cl_2 ; k) 2-azidoethanamine; l) NaBH(OAc)_3 (66%); m) PMe_3 , NaOH; n) Na/NH_3 , THF (65%).

followed by nucleophilic substitution with sodium azide to yield compound **15**. Allylation of the 4'-hydroxy group with allyl bromide in the presence of NaH in DMF gave 4'-allyl derivative **16**. Attempts to convert **16** into the corresponding aldehyde by ozonolysis resulted in a mixture of products owing to partial oxidation of the benzyl groups. To solve this problem, the double bond in **16** was first converted into corresponding diol **17** by using the procedure of Nicolaou.^[24] Oxidative cleavage of diol **17** [PhI(OAc)_2 , CH_2Cl_2] was followed by in situ reductive amination with 2-azidoethanamine^[25] to yield corresponding 4'-azido amine **18** in 66% yield. Finally, after several unsuccessful attempts to remove the benzyl and azide protections in **18**, we found that a sequential operation involving Staudinger and Birch reactions was the best protocol. Thus, the Staudinger reaction (PMe_3 , NaOH) followed by Birch reduction (Na/NH_3 , THF) gave target compound **1** in 65% yield.

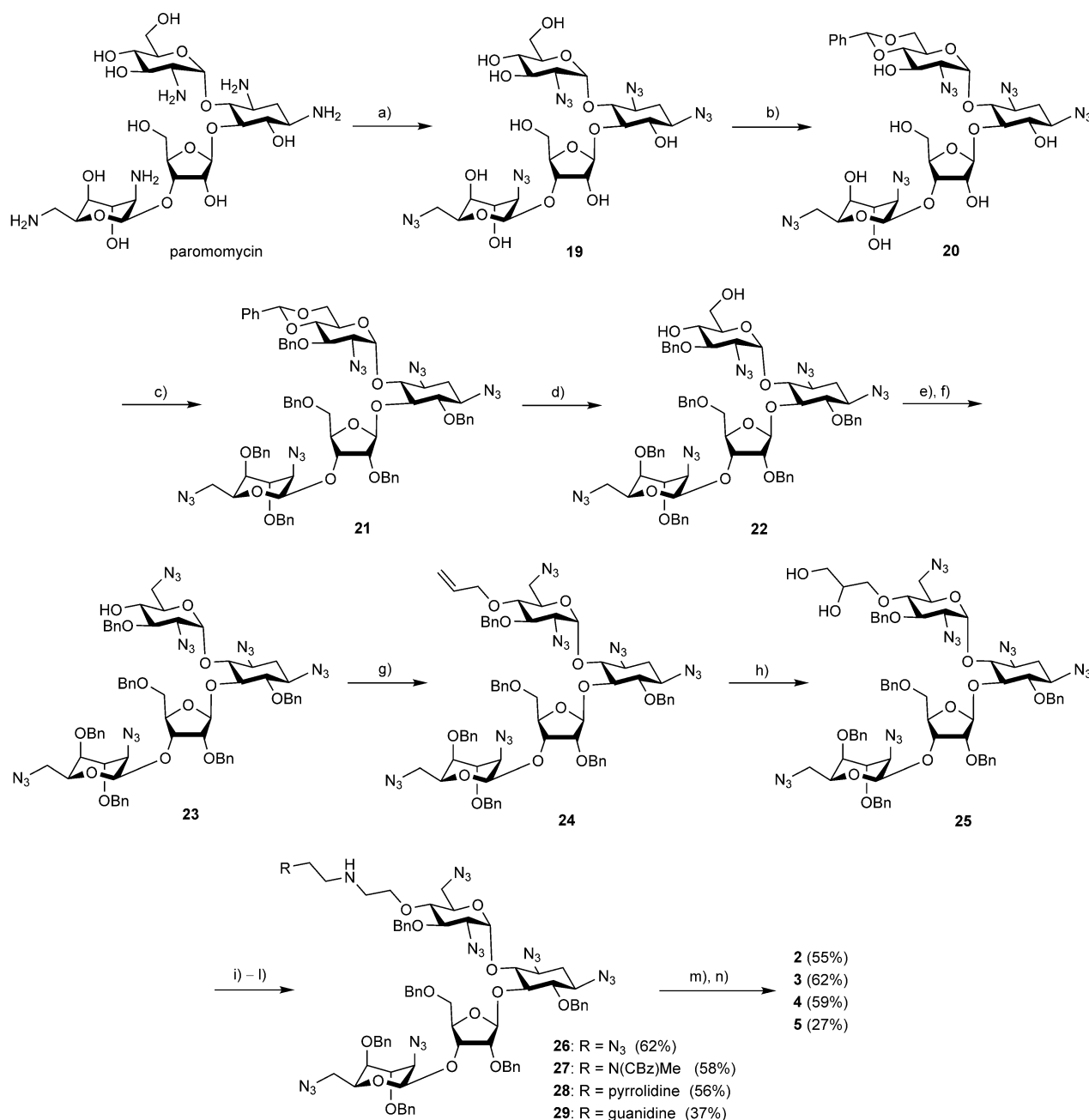
The 4'-O-substituted derivatives of NeoB, compounds **2–5** (Scheme 1), were synthesized by using the same strategy as that described for the synthesis of compound **1** with some modifications, as illustrated in Scheme 3. The modifications used were as follows. Unlike the azidation of paromamine with TfN_3 to yield corresponding perazido derivative **11** (Scheme 2), the same reaction on paromomycin gave a very low yield of desired perazido derivative **19**.^[26,27] In an attempt to improve the yield of the desired perazido product, instead of TfN_3 we used imidazole-1-sulfonyl azide hydrochloride ($\text{ImSO}_2\text{N}_3\cdot\text{HCl}$)^[28]

and replaced tosyl chloride with the more bulky triisopropylsulfonyl chloride (trisyl chloride), which was more selective for protection of the 6'-hydroxy group (conversion of compound **22** into **23**) and gave 60% yield over two steps (trisylation and azidation).

Common intermediate diol **25** was separately subjected to in situ oxidation and reductive amination steps with four different amine linkers, compounds **A**, **B**, 1-(2-aminoethyl)pyrrolidine, and **C**,^[25] to afford the corresponding protected 4'-O-



derivatives of NeoB, compounds **26–29** (Scheme 3). The Staudinger reaction (PMe_3 , NaOH) followed by the Birch reduction (Na/NH_3 , THF) gave target compounds **2–5** in average-to-modest yields. The structures of new compounds **1–5** were all confirmed by combining various 1D and 2D NMR spectroscopy techniques, including 2D ^1H - ^{13}C HMQC and HMBC, 2D COSY, and 1D selective TOCSY experiments, along with mass spectrometry analysis.

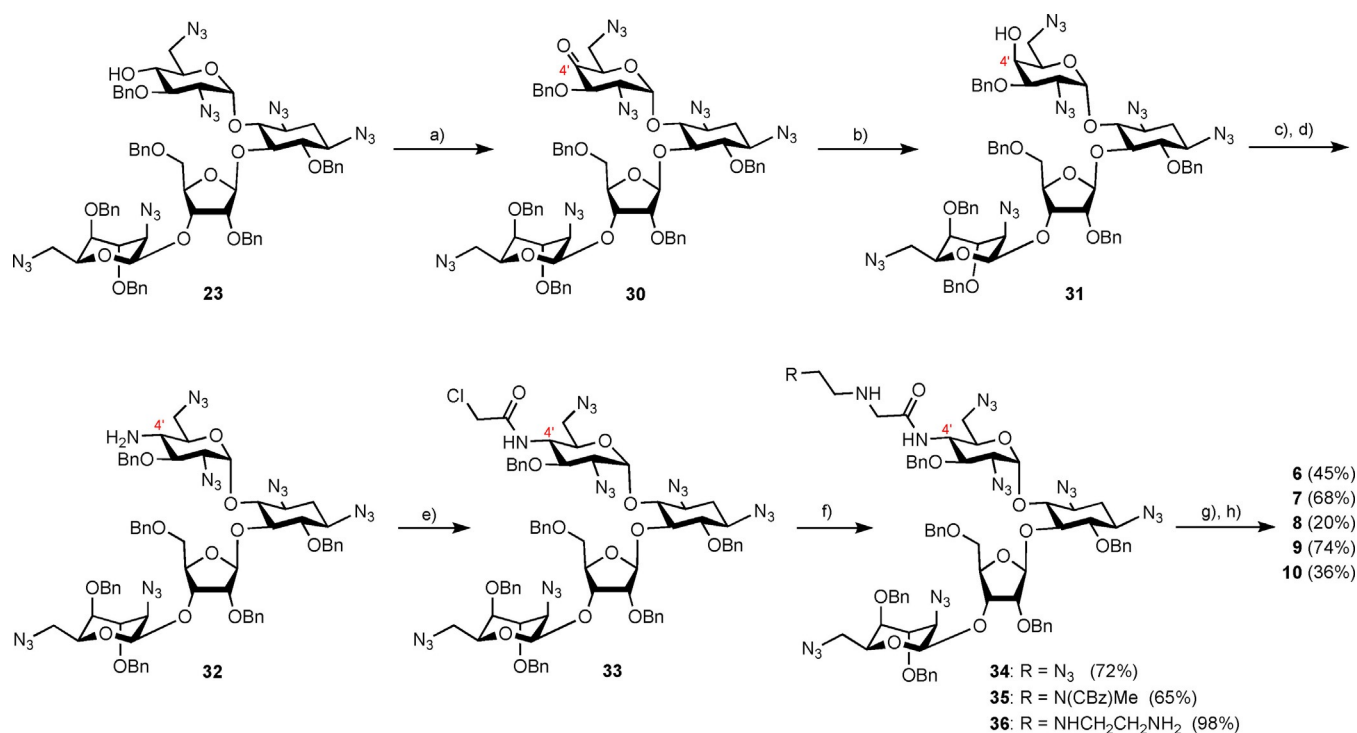


Scheme 3. Chemical transformation of paromomycin into synthetic derivatives 2–5. a) $\text{ImSO}_2\text{N}_3\cdot\text{HCl}$, CuSO_4 (70%); b) PhCH(OMe)_2 , CSA, DMF (88%); c) BnBr , NaH , DMF (60%); d) $\text{AcOH}/\text{H}_2\text{O}$ (61%); e) Trisyl chloride, py; f) NaN_3 , DMF (60%); g) allyl bromide, NaH , DMF (92%); h) K_2OsO_4 , NMO, acetone/ H_2O (89%); i) PhI(OAc)_2 , CH_2Cl_2 ; j) amines A, B, 1-(2-aminoethyl)pyrrolidine, C; k) NaBH(OAc)_3 ; l) trifluoroacetic acid, CH_2Cl_2 ; m) PME_3 , NaOH ; n) Na/NH_3 , THF.

Synthesis of 4'- and 6'-amide-linked compounds

For the synthesis of the 4'-amide derivatives, alcohol **23** (Scheme 4) was first oxidized with Dess–Martin periodinane (DMP) to form corresponding 4'-ketone **30**, which was then reduced with sodium borohydride to afford compound **31** with an axial hydroxy group at the 4'-position. Compound **31** was treated with triflic anhydride (Tf_2O , pyridine, CH_2Cl_2) to form the corresponding 4'-triflate, which was then treated with ammonia in acetone to yield **32** with an equatorial amine group at the 4'-position. Next, **32** was treated with chloroacetyl chlo-

ride to give 4'-chloride **33**, which was then separately treated with three different amines, compounds A and B and diethylenetriamine, to afford the corresponding 4'-amide derivatives of NeoB in their protected forms (compounds **34**, **35**, and **36**, respectively). These products were then deprotected by using the two-step procedure described above (Staudinger and Birch) to afford the corresponding 4'-amide derivatives of NeoB, compounds **6**, **7**, and **8**, in yields of 64, 68, and 20%, respectively (Scheme 4). Interestingly, during the last deprotection step (the Birch reduction), we discovered that if this step was performed in the presence of an excess amount of



Scheme 4. Chemical transformation of intermediate **23** into synthetic derivatives **6–10**. a) DMP, CH₂Cl₂ (86%); b) NaBH₄, MeOH (82%); c) Tf₂O, py/CH₂Cl₂; d) acetone/ NH₃ (41%); e) chloroacetyl chloride, NaHCO₃, THF (98%); f) amines A, B, diethylenetriamine; g) PMe₃, NaOH; h) Na/NH₃, THF; CBz = benzyloxy-carbonyl.

sodium, transamidation rearrangement of the warhead, from the 4'-position to the 6'-position, took place. The structure of the rearrangement product (6'-amide) was confirmed by its isolation and subsequent spectral assignment by using a combination of various 1D and 2D NMR spectroscopy techniques (see Figure S1 in the Supporting Information). This rearrangement probably occurred as a result of the strong basic conditions generated after quenching of the reaction, which resulted in the formation of sodium hydroxide. We exploited this transformation by performing the Birch reaction step with an excess amount of sodium and synthesized corresponding 6'-amide-linked compounds **9** and **10** in yields of 74 and 36%, respectively.

Antibacterial activity and protein translation inhibition tests

To probe the influence of the attached warheads on antibacterial activity, the minimal inhibitory concentration (MIC) values for new designer structures **1–10** were determined against wild-type (WT) Gram-negative and Gram-positive bacteria. Although this simple test cannot confirm or disprove catalytic activity, it is nonetheless of utmost importance, as it reveals how the compounds act in vivo. Furthermore, we anticipated that unusually low MIC values would be indicative of a high catalytic rate and turnover.

Table 1 shows the comparative MIC values of NeoB and compounds **1–10** against both Gram-negative and Gram-positive bacteria, including pathogenic and resistant strains. The bacterial strains that were included in these tests were as fol-

lows: two WT *E. coli* strains (R477-100 and 25922) as representatives of Gram-negative bacteria with unknown resistance to aminoglycosides^[29] and two WT *Staphylococcus epidermidis* and *Bacillus subtilis* strains as representatives of Gram-positive bacteria (the clinically used aminoglycosides have significant antibacterial activity against these strains).^[30] The resistant strains included MRSA, a Gram-positive bacterium, the treatment of which represents a great challenge in the clinic; MRSA 252, which is known for its high resistance to aminoglycosides,^[31] and MRSA CI 15877, which is resistant to natural aminoglycosides.^[32] Other pathogens that were tested included several strains of *P. aeruginosa* that have an inherent resistance to aminoglycosides.^[33,34]

The comparative data collected in Table 1 show that all the new derivatives of NeoB, compounds **2–10**, exhibit significant antibacterial activity against both the WT and aminoglycoside-resistant strains, including Gram-negative and Gram-positive bacteria. In general, the activity of the novel NeoB derivatives against the WT Gram-negative bacteria is similar to or slightly lower than that of the parent NeoB. The activities against the WT Gram-positive bacteria were diverse across the different strains tested. The activity of most of the compounds against *S. epidermidis* is similar to or better than that of NeoB, whereas the activity against *B. subtilis* is generally lower than that of NeoB. Interestingly, all new derivatives (compounds **2–10**) show significantly improved activity against the Gram-negative strains of pathogenic *P. aeruginosa* in comparison with NeoB. *P. aeruginosa* is a nosocomial human pathogen known to be inherently resistant to aminoglycosides owing to the presence

Table 1. Comparative antibacterial activity (MIC values) and inhibition of protein translation (IC_{50} values) in the prokaryotic system of NeoB and synthetic compounds **1–10**.^[a]

Compd.	Gram-negative		Gram-positive		MIC [$\mu\text{g mL}^{-1}$]			MRSA		<i>Geobacillus</i>		IC_{50} [μM]
	a	b	c	d	<i>P. aeruginosa</i> e	f	g	h	i	j	k	
NeoB	12	12	6	0.75–1.5	> 192	48–96	192	> 192	48	0.2	12	0.01 ± 0.002
1	384	> 384	192	48	48–96	48–96	48–96	192	48	6	12	2.03 ± 0.3
2	48	48	6	6	24–48	6–12	24	6–12	0.75	0.2	0.8	0.02 ± 0.001
3	96	96	6	6–12	48	12	24	24	3	0.2	0.8	0.03 ± 0.005
4	48	48–96	6	3–6	96	48	48	24	6	0.2	0.8	0.03 ± 0.007
5	192	192	24	12	–	–	–	–	–	–	–	0.08 ± 0.005
6	24	48	6	2	24	6	48	24–48	1.5	0.2	0.4	0.005 ± 0.0005
7	24	24	6	3–6	24	24	48	24	1.5	0.2	0.4	0.07 ± 0.004
8	48	48	3	6	24	24–48	48	12–24	0.75	0.4	1.5	0.07 ± 0.007
9	48	48	6	3–6	48	48–96	24	12	1.5	0.2	0.8	0.006 ± 0.0009
10	24	48	6	3	24	24	48–96	12–24	1.5	0.2	0.4	0.006 ± 0.0009

[a] The rows in bold highlight the most potent compounds. a: *E. coli* R477-100; b: *E. coli* 25922; c: *S. epidermidis*; d: *B. subtilis*; e: *P. aeruginosa* 1275; f: *P. aeruginosa* 27853; g: *P. aeruginosa* O1; h: MRSA 252; i: MRSA 15877; j: *Geobacillus stearothermophilus* T-1 60 °C; k: *Geobacillus stearothermophilus* KanR 60 °C.

of the chromosomally encoded APH(3')-IIb enzyme. This enzyme catalyzes the transfer of the ATP γ -phosphoryl group to the 3'-hydroxy group of many aminoglycosides, rendering them inactive as antibiotics.^[34] The observed improved activity of the new derivatives relative to that of NeoB against the tested strains of *P. aeruginosa* can be explained by the steric hindrance of the cationic warhead, which introduces unfavorable interactions with the APH(3')-IIb enzyme active site.

A very similar improvement in antibacterial performance of the new designers versus that of NeoB was also observed against the Gram-positive pathogenic MRSA strains. Specifically, large improvements were observed for compounds **2** and **8**, which exhibited MIC values that were 64 times lower than that of NeoB. No significant difference in antibacterial activity was observed between the 4'-ether (compounds **1–5**) and 4'-amide (compounds **6–8**) derivatives, even though we expected the 4'-amide derivatives to be more active because of the potential for additional attractive interactions between the amide bond and the rRNA. The antibacterial activity of compound **1**, a neamine-based derivative, is substantially lower than that of the other compounds tested, indicating that its binding affinity to the A-site is much lower.

Given that the successful cleavage of an RNA phosphodiester bond requires substantial conformational flexibility, it was important to investigate the possibility that the standard incubation temperature of 37 °C was not high enough to allow the "installed warheads" to reach the activation energy required for hydrolysis of the scissile phosphodiester bond of rRNA. To test this hypothesis, we decided to test the antibacterial activity against the thermophilic strain *Geobacillus T1* with the optimal growth temperature of 60 °C (Table 1). We expected that if the new compound had catalytic activity, it would show better activity than NeoB at 60 °C. However, new compounds **1–10** all showed antibacterial activity similar to that of NeoB against the WT *Geobacillus T1*. Against the *Geobacillus T1* harboring the resistance to kanamycin, as expected, most of the new

compounds maintained their high antibacterial activity, whereas NeoB almost lost its activity.

In summary, even though we cannot conclude from the observed comparative MIC data whether or not compounds **1–10** have catalytic activity, we can definitely claim that the modifications we introduced did not hinder binding to the A-site and that most of the derivatives retained significant antibacterial activity. Moreover, the new compounds overcame the existing resistance of *P. aeruginosa* and MRSA pathogens to aminoglycosides, which is one of the greatest challenges in today's antibacterial research.

Next, we tested the protein translation inhibition by determining half-maximum inhibition levels (IC_{50} values, Table 1). Whereas most of the new compounds showed activity of the same order of magnitude as the parent NeoB, the inhibitory potency of compounds **6**, **9**, and **10** with a 4'-nitrogen atom was twofold higher than that of NeoB (IC_{50} values of 0.006, 0.005, 0.006, and 0.01 for **6**, **9**, **10**, and NeoB, respectively). This could be explained by the additional interactions of the 4'-amide (compound **6**) and 4'-amine (compounds **9** and **10**) groups of these compounds with the ribosomal A-site. However, the increased binding affinity of the compound for the A-site may result in its slow dissociation from the ribosome (very small k_{off} value), which would then adversely affect the catalytic performance. To test this possibility, we synthesized compound **1**, which is a smaller analogue of compound **2**, as it lacks rings III and IV of NeoB. We found that the inhibition potency of compound **1** (IC_{50} = 2.03 μM , a neamine derivative) was two orders of magnitude lower than that of the other compounds tested and was one order of magnitude lower than that of the parent neamine scaffold (IC_{50} = 0.28 μM). Thus, it would appear that the neamine pharmacophore is not a suitable choice for the aminoglycoside scaffold, unless the catalytic efficiency of the warhead is greatly improved, as attachment of the warheads has a deleterious effect on the binding affinity at the target.

RNase activity tests

Given that compounds **1–10** did not show substantially higher antibacterial activity than NeoB against WT bacteria, we decided to directly assess the potential RNase activity of these compounds by using gel electrophoresis experiments, as previously reported for ColE3.^[20] We envisioned that by incubating the designer structures with the complete 70S ribosomes, the isolated 30S ribosomal particles, or the synthetic A-site oligonucleotide model structures we could determine whether the new compounds have catalytic activity.

Initially, the experiments were performed on full-size ribosomes isolated from *E. coli*, as previously reported.^[35] As a positive control, we used the RNase domain of the natural toxin ColE3 obtained from Prof. Colin Kleanthous from Oxford University (Figure 2B). As expected, with ColE3 we observed cleavage of approximately 40 bases from the 16S rRNA fragment (≈ 1540 nucleic bases) in a dose-dependent manner. Figure 2 also shows the 5S and tRNA fragments. However, the experiments with NeoB and compound **3** (Figure 2C,D) did not show any signs of the cleaved product at concentrations up to 400 μM . At higher concentrations, we encountered solubility problems, which prevented us from detecting RNA cleavage. Within the same concentration range (up to 400 μM), ethylenediamine (a negative control) did not cleave the full ribosome (Figure 2A), suggesting that it is unable to bind to rRNA effectively.

To avoid precipitation and to allow the use of higher concentrations of aminoglycosides, instead of ribosomal particles, we decided to use an A-site oligonucleotide model. We selected an oligonucleotide model similar to that used by Westhof and co-workers^[36,37] for crystallographic studies. To improve RNA detection, we added a fluorescent Cy3 tag at the 3' end (and not at the 5' end) to ensure that there was a significant difference between the size of the full-length RNA and the cleaved RNA (Figure S2). The cleavage experiments indicated that with ethylenediamine (N-2-N) we observed nonspecific cleavage only at high concentrations, 100 and 200 μM of N-2-N (Figure 3A).

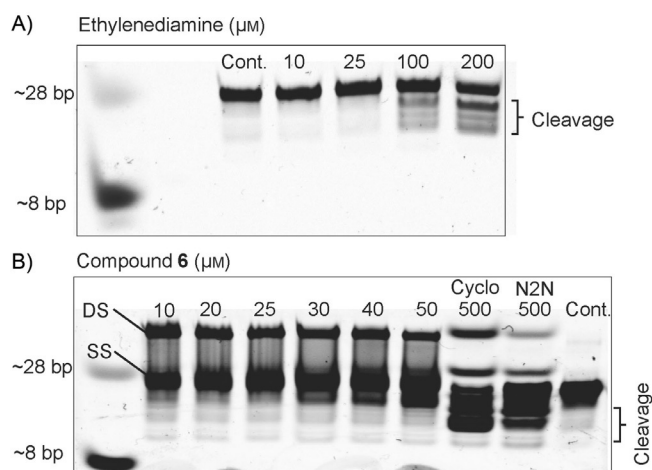


Figure 3. Cleavage experiments of the A-site oligonucleotide model rRNA (23 bases labeled at 3' with the fluorescent Cy3 tag, incubated for 24 h, pH 8, 37 °C; for the sequence of rRNA see Figure S2) in the presence of ethylenediamine and compound **6**. A) Lane 1: RNA markers; lane 2: blank lane; lane 3: not treated (control); lanes 4–7: rRNA oligonucleotide treated with increased concentrations of ethylenediamine. B) Lane 1: RNA markers; lanes 2–7: rRNA oligonucleotide treated with increased concentrations of compound **6**; lanes 8 and 9: rRNA oligonucleotide treated with 500 μM 1,2-cyclohexanediamine (Cyclo) and ethylenediamine (N2N), respectively; lane 10: not treated (control). rRNA fragments were analyzed on 20% TBE/urea gel and were visualized by fluorescence. DS: double-stranded rRNA; SS: single-stranded rRNA.

In the presence of compound **6**, we detected some RNA cleavage at substantially lower concentrations, 10 μM (Figure 3B). We observed double-stranded RNA (DS band in Figure 3B), which suggested that aminoglycoside binding stabilized double-stranded RNA even though the gel was under denaturing conditions. In addition, only nonspecific cleavage bands were observed at the concentrations tested, and these fragments were far longer than those expected for specific and selective cleavage (< 8 bases).

All in all, we conclude that the initial NeoB derivatives (compounds **1–10**) that we designed and tested exhibit significant

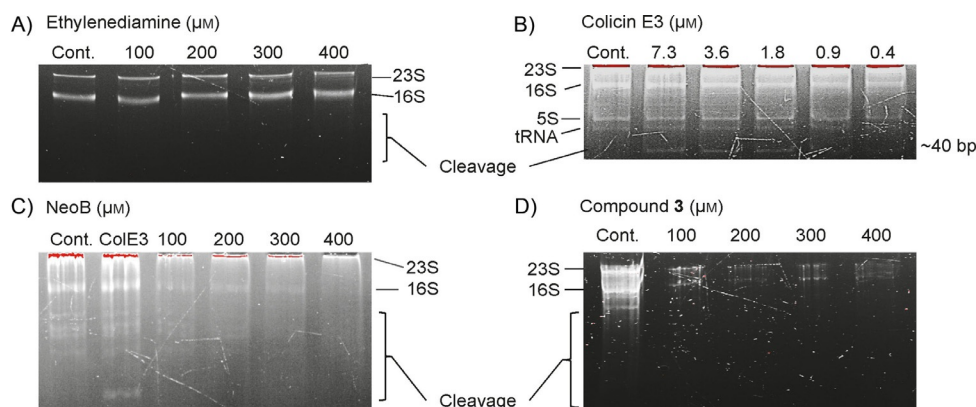


Figure 2. Cleavage experiments of *E. coli* ribosomes in the presence of ethylenediamine, colicin E3, NeoB, and compound **3**. A) Lane 1: *E. coli* ribosomes (control); lanes 2–5: ribosomes treated with increasing concentrations of ethylenediamine. B) Lane 1: control; lanes 2–6: ribosomes treated with decreased concentrations of colicin E3. C) Lane 1: control; lane 2: ribosomes treated with 7.3 μM colicin E3 (ColE3); lanes 3–6: ribosomes treated with increasing concentrations of NeoB. D) Lane 1: control; lanes 2–4: ribosomes treated with increasing concentrations of compound **3**. rRNA fragments were analyzed on 6% acrylamide TBE/urea gel, stained with SYBR Gold and were analyzed by fluorescence.

antibacterial activity and overcome existing resistance to aminoglycosides; however, they lack any significant catalytic activity, as we would have expected according to our initial design strategy.

MD simulations

Conformational dynamics of the warheads and the possibility of RNA cleavage: In an attempt to explain the experimental data of newly designed compounds **1–10** at the molecular level, we performed full-atom molecular dynamics (MD) followed by Gaussian accelerated MD (GaMD).^[38,39] The crystal structure of NeoB bound to the oligonucleotide model of the A-site rRNA (PDB ID: 2ET4)^[19] was used as a template for building the systems used in the simulations (for details see Simulation Methods in the Supporting Information, Figure S6). Four representative derivatives of NeoB, compounds **2**, **5**, **8**, and **10**, were simulated, and NeoB was used as a control. The total MD and GaMD simulation time was about 5.5 μ s.

For compounds **2** and **5**, we found two and three different conformations of the warheads, respectively (Figures S3 and S4). For both, the dominant conformation of the warhead (82.7% of the population in **2** and 76.4% of the population in **5**) is characterized by a common intramolecular hydrogen bond between the N1 amine of the warhead and the N6' ammonium of the aminoglycoside ring I. Unfortunately, these intramolecular hydrogen bonds prevent the N1 amine of the warhead from acting as the general base to activate the 2'-OH group of the G1491 ribose as a nucleophile (see Figure 1 for the proposed mechanism).

In contrast to **2** and **5**, the warhead of **8** and **10**, which represent the 4'- and 6'-amide derivatives of NeoB, is longer and does not form any similar intramolecular interactions with the rest of the molecule (Figures 4 and S5). For compound **10** (Figure S5), we observed that the largest conformational variability of the warhead is associated with its rotation around the N2–C3–C4–N3 dihedral angle. Therefore, we used this coordinate in the clustering analysis and found two major conformations of the warhead (72.2 and 27.8% of the population). The short-range contacts of the N4' ammonium with the phosphates of A1492 and A1493 conformationally restrict not only the position of ring I in the A-site but also the A1492 and A1493 backbone atoms.

For compound **8**, we identified three principal modes of binding of the warhead to the rRNA (Figure 4). In the most-abundant binding mode (58.6% of the population), we observed two short-range interactions between the 2'-hydroxy group of the ribose (G1491) and the N3 amine group of compound **8** (proposed general base) and between the A1492 phosphate and the N4 ammonium of compound **8** (general acid). Importantly, this conformational state of compound **8** is consistent with the hypothetical mechanism of A-site rRNA cleavage between G1491 and A1492 (Figure 1). In the second-most-abundant binding mode of compound **8** (21.6% of the population), the N2 amine group forms a hydrogen bond with the 2'-hydroxy group of the ribose of G1491, which actually serves as the general base. However, the concomitant stabiliza-

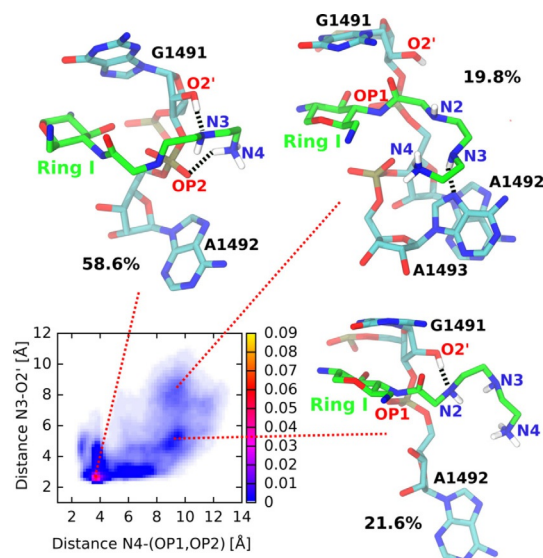


Figure 4. The normalized occurrence of the three binding modes of compound **8** warhead to A-site as a function of the two intermolecular distances N3–O2' and N4–(OP1, OP2). The representative structures are presented. For clarity, only ring I of the aminoglycoside (in green) and hydrogen atoms crucial for interactions of the warhead are shown. Black dashed lines denote donor–acceptor short-range interactions.

tion of the transition state through the interaction of the warhead amines with the phosphate of A1492 is lacking, and this would significantly limit the efficiency of hydrolysis.

Considering the formation of the interactions required for A-site rRNA cleavage between G1491 and A1492, compound **8** seems to be the best candidate among the selected derivatives for the development of a catalytic antibiotic. The N3 amine of the warhead activates the 2'-OH group of the G1491 ribose for nucleophilic attack, and the N4 ammonium of the warhead favorably binds to the OP2 and O3' atoms of the A1492 phosphate, which facilitates nucleophilic attack. However, the warhead hardly interacts with the O5' atom, and consequently, activation of the leaving group would be minimal. We therefore predict that elongating the warhead might be beneficial so that the N4 ammonium could interact with the A1492 phosphate leaving group more directly and frequently.

In general, the efficiency of rRNA hydrolysis is highly dependent on the ability of the catalyst to induce the correct positioning of the nucleophile for in-line attack on the scissile bond. Enzymes, being large, can mechanically achieve this step “easily” by distorting the substrate to reach the conformation necessary for efficient catalysis. For example, ColE3^[20] and α -sarcin,^[40] the two bacterial toxins that cleave a single phosphodiester bond of rRNA (in the small and large ribosomal subunits, respectively), both use RNA base flipping to dock the substrate into the active site in such a manner so as to facilitate crucial in-line attack. Whether the aminoglycoside–warhead combination can induce a similar conformational change in the rRNA A-site is one of the most important questions of this work. To address this question, we measured the angle created between the 2'-OH (the G1491 ribose, the nucleophile),

the phosphorus of the phosphate between G1491 and A1492, and the 5'-O (the leaving group)—O—P—O angle.

In the crystal structure of the Westhof model that we used for the simulations, the O—P—O angle does not exceed 90°. Figure 5 compares the distributions of the O—P—O angle, as obtained from GaMD simulations of NeoB and derivatives **2**, **5**, **8**,

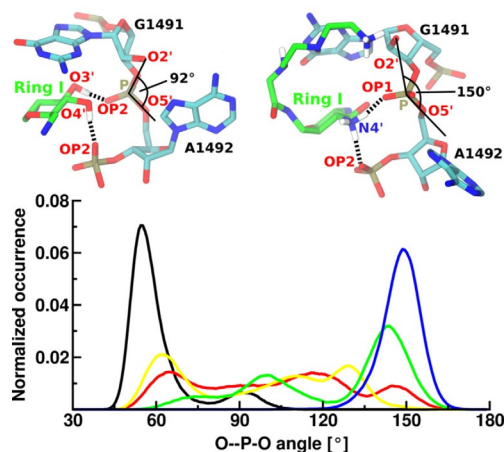


Figure 5. Distributions of the O—P—O angle for NeoB (—) and compounds **2** (—), **5** (—), **8** (—), and **10** (—) in GaMD simulations. Above is shown the O—P—O angle in the representative structures of NeoB (left) and compound **10** (right). The donor–acceptor short-range interactions important for stabilization of the O—P—O angle are marked by black dashed lines. For clarity, only ring I of the aminoglycosides (in green) and selected hydrogen atoms are shown.

and **10**. The smallest values of this angle are found for the NeoB complex, distributed in the range of 45 to 105°. The interactions formed between O3' of NeoB (ring I) and OP2 of the A1492 phosphate and between O4' of NeoB (ring I) and OP2 of the A1493 phosphate seem to be the most important for orientation of the O—P—O angle. The modifications introduced into NeoB ring I to make compounds **8** and **10** clearly lead to an increase in this angle for both derivatives, reaching as high as 170° for **10**. We found that for the nearly linear orientation of the O—P—O angle, a strong and stable interaction with the OP1 atom of the A1492 phosphate is essential. For compound **8**, this requirement is fulfilled thanks to the persistent hydrogen bond formed by the 3'-hydroxy group of ring I and concomitant stabilization of the A1492 phosphate by the N4 ammonium group of the warhead. For compound **10**, the crucial short-range interaction with the OP1 atom of the A1492 phosphate is made by the N4' ammonium in ring I. Even though the warhead of compound **10** does not reach the putative rRNA cleavage site, stabilization of the O—P—O angle in the nearly in-line orientation is remarkable. Thus, we believe that by using flexible docking algorithms the structure of the warhead of compound **10** can be remodeled to optimize its ability to form the interactions necessary to cleave the rRNA. Therefore, together with compound **8**, we consider **10** as a lead compound for the next generation of new aminoglycoside derivatives that are designed to achieve rRNA catalysis.

Summary and Conclusion

We adopted the idea of catalytic antibiotics from nature: bacteria produce bacteriocins that exert their lethal action by an enzymatic nuclease digestion mechanism. On the basis of the most recent structural and mechanistic data on the bacteriocin ColE3 and on aminoglycoside antibiotics, we designed and synthesized a series of aminoglycosides bearing a potential catalytic moiety, with the expectation that these molecules could mimic ColE3 activity. Our design principles included a careful analysis of the choice of the “target” phosphodiester bond, the “catalytic warhead” structures, and the attachment site on the aminoglycoside scaffold. We selected the phosphodiester bond between the rRNA bases G1491 and A1492 as the potential cleavage site and the 4'-OH group (ring I) of the natural aminoglycoside NeoB as an attachment site for the catalytic warheads, and by attaching a series of different 1,2-diamines as potential catalytic warheads, we prepared new NeoB derivatives (compounds **1–10**, Scheme 1).

To probe the influence of the attached warheads on antibacterial activity, derivatives **1–10** were tested against WT, pathogenic, and aminoglycoside resistant strains (Table 1). In general, compounds **2–10** showed significant antibacterial activity against WT bacteria, and it was similar to or slightly lower than that of the parent NeoB. The observed antibacterial data was corroborated by in vitro protein translation inhibition data (IC₅₀ values, Table 1), showing activity similar to that of the parent NeoB. Of particular note was the potent antibacterial activity of the new derivatives (relative to that of NeoB) against resistant and pathogenic strains such as *P. aeruginosa* and MRSA, and the lead compounds exhibited MIC values that were eight to 16 times lower in *P. aeruginosa* (compound **6**) and 64 times lower in MRSA (compounds **2** and **8**).

We anticipated that unusually low MIC and IC₅₀ values against WT bacteria would be indicative of significant catalytic activity on the ribosomal RNA, but in this regard, the observed data was not encouraging. However, these data alone cannot conclusively disprove the desired hydrolytic activity, as they could also be explained by a low catalytic turnover resulting from strong binding affinity of the derivative to the cleaved rRNA.

To address whether the new derivatives exhibited the anticipated hydrolytic activity, we tested the comparative RNase activity by using full-size ribosomes isolated from *E. coli* (Figure 2) and the bacterial A-site oligonucleotide model RNA (Figure 3). In the *E. coli* ribosomes, we confirmed the reported activity of the ColE3 as the positive control. However, neither NeoB nor compound **3** showed any activity at concentrations up to 400 μM; at higher concentrations, we encountered solubility problems. The cleavage experiments with the A-site oligonucleotide model RNA indicated weak, dose-dependent but nonspecific hydrolytic cleavage activity for compound **6**. Although other RNA models could be employed that would more precisely monitor strand cleavage (e.g., the use of a ³²P end-labeled A-site RNA construct^[41]), it is clear that if the new derivatives would exhibit the desired function at an appreciable level, the experiments we performed would certainly

detect them. In view of these discouraging results, it is prudent to consider whether or not there is sufficient justification to encourage further research towards catalytic aminoglycosides and, if so, what the next step should be.

The fact that the observed MIC and IC_{50} values of **2–10** were similar to those of NeoB against WT bacteria indicated that the modifications on NeoB did not hinder bacterial cell permeability or the binding affinity of the aminoglycoside scaffold to the target site. Furthermore, full-atom GaMD simulations (Figure 5) on the crystal structure of NeoB bound to the oligonucleotide model of the A-site rRNA revealed that the O–P–O angle for compounds **8** and **10** was significantly greater than that for NeoB (between 45 and 105°), reaching as high as 170° for **10**; this is remarkably close to the ideal, in-line orientation for nucleophilic attack. These data support the notion that appropriately designed aminoglycoside warheads such as **8** and **10** have the capacity, one, to bind selectively to the regular aminoglycoside binding site and, two, to induce the conformational changes that are necessary to lower the activation barrier of the transition state for hydrolytic cleavage. Taken together, these results suggest that by using flexible docking algorithms, the structures of the warheads in compounds **8** and **10** could be remodeled to optimize their ability to catalytically cleave the rRNA.

In summary, this pilot study provides a new direction for the development of novel aminoglycoside-based small molecules that target bacterial rRNA by means of optimizing the efficacy of aminoglycoside-induced rRNA cleavage; this progress may offer promise for the development of catalytic antibiotics as a new paradigm in antibiotics research. Thus, although a “catalytic aminoglycoside” has yet to be found, the results introduced in this study indicate that this is an achievable goal. More comprehensive design strategies are now being employed, and they incorporate advanced molecular dynamics techniques and more powerful metal-free and metal-based catalytic warheads to optimize the catalytic activity of the new designer structures.

Experimental Section

General techniques: NMR spectra (including 1H , ^{13}C , DEPT, 2D COSY, 1D TOCSY, HMQC, HMBC) were routinely recorded with a Bruker Avance 500 spectrometer, and chemical shifts are reported relative to internal Me_4Si ($\delta = 0.0$ ppm) with $CDCl_3$ as the solvent or to MeOD ($\delta = 3.35$ ppm) as the solvent. ^{13}C NMR spectra were recorded with a Bruker Avance 500 spectrometer at 125.8 MHz, and the chemical shifts are reported relative to the solvent signal for $CDCl_3$ ($\delta = 77.00$ ppm) or to the solvent signal for MeOD ($\delta = 49.0$ ppm). Mass spectra analyses were obtained with a Bruker Daltonix Apex 3 mass spectrometer under electrospray ionization (ESI) or a TSQ-70B mass spectrometer (Finnigan Mat). Reactions were monitored by TLC on Silica Gel 60 F_{254} (0.25 mm, Merck), and spots were visualized by charring with a yellow solution containing $(NH_4)_2Mo_7O_{24} \cdot 4H_2O$ (120 g) and $(NH_4)_2Ce(NO_3)_6$ (5 g) in 10% H_2SO_4 (800 mL). Flash column chromatography was performed on Silica Gel 60 (70–230 mesh). All reactions were performed under an argon atmosphere with anhydrous solvents, unless otherwise noted. Neomycin B and paromomycin as analytical samples for comparative biochemical assays were purchased from Sigma. For

chemical syntheses, large-scale paromomycin (used as a starting material) was purchased from Apollo Scientific (Stockport, UK). All other chemicals and biochemicals, unless otherwise stated, were obtained from commercial sources. In all biological tests, all the tested aminoglycosides were in their sulfate salt forms, except compound **5**, which was used as its trifluoroacetate salt.

Biochemical assays: Prokaryotic in vitro translation inhibition by the different standard and synthetic aminoglycosides was quantified in coupled transcription/translation assays by use of *E. coli* S30 extract for circular DNA with the pBEST/luc plasmid (Promega), according to the manufacturer's protocol. Translation reactions (25 μ L) containing variable concentrations of the tested aminoglycoside were incubated at 37 °C for 60 min, cooled on ice for 5 min, and diluted with a dilution reagent [Tris-phosphate buffer (25 mM, pH 7.8), dithiothreitol (DTT, 2 mM), 1,2-diaminocyclohexanetetraacetate (2 mM), glycerol (10%), triton X100 (1%), and bovine serum albumin (BSA, 1 mg mL $^{-1}$)] into 96-well plates. The luminescence was measured immediately after the addition of Luciferase Assay Reagent (Promega) (50 μ L), and light emission was recorded with a Victor3 Plate Reader (PerkinElmer). The concentration of half-maximal inhibition (IC_{50}) was obtained from fitting concentration–response curves to the data of at least three independent experiments by using Grafit 5 software.^[42]

Comparative antibacterial activities were determined by measuring the MIC values by using the double-microdilution method according to the National Committee for Clinical Laboratory Standards (NCCLS).^[43] All the experiments were performed in triplicate, and analogous results were obtained in three different experiments.

For the rRNA cleavage experiments, the ribosomes were isolated from *E. coli* cells (R477-100) by following the reported protocol.^[35] Ribosomes were pelleted from pooled fractions (35 K for 15 h at 4 °C) and were resuspended in buffer for snap freezing in liquid nitrogen and storage at -80 °C. The resin was rinsed with water after use and was stored in 20% ethanol at 4 °C. The catalytic domain of ColE3 (provided by Prof. Colin Klenathous, University of Oxford, UK) was purified from its immunity protein as previously described.^[44] Briefly, after elution from the Ni-affinity column with 6 M Gn-HCl, the ColE3 RNase became unfolded. It refolded upon dialysis in 50 mM potassium phosphate or 20 mM Tris pH 7.5 buffer. All parts of the purification procedure could be performed at room temperature, and the product was analyzed on 16% SDS-PAGE.

The cleavage experiments of rRNA with *E. coli* ribosomes were performed by incubation of freshly isolated ribosomes for 24 h (5 min in the case of ColE3; 37 °C, pH 7.0) in the presence of ethylenediamine, NeoB, compound **3**, or ColE3. After incubation, RNA was phenol/chloroform extracted from samples and was electrophoresed on a 6% acrylamide TBE/urea gel for 100 min at 180 V, stained with SYBR Gold, and analyzed by fluorescence. A short RNA oligomer that represented the bacterial A-site sequence labeled with a fluorescent tag (23 bases, for sequence see Figure S2) was also used for rRNA cleavage experiments. This RNA sequence was purchased from Dharmacon and was used without further purification. The cleavage experiments were performed by using gel electrophoresis; the rRNA fragments were analyzed on 20% TBE/urea gel and were visualized by fluorescence.

Molecular dynamics simulations: MD simulations were performed on the model of the A-site containing two symmetric aminoglycoside binding sites by using the crystal structure of the A-site with neomycin B bound (PDB ID: 2ET4).^[19] The MD simulation protocol consisted of energy minimization, thermalization, equilibration, and production phases. In the first two phases, harmonic con-

straints with a force constant of $10 \text{ kcal mol}^{-1} \text{ \AA}^{-2}$ were imposed on heavy atoms of the solute. First, all systems were energy minimized with the above restraints undergoing 5000 steps of steepest descent followed by 4000 steps of conjugate gradient minimization by using *sander* (Amber 12). The next phases were performed with NAMD.^[45] Second, during thermalization (in the NVT ensemble), each system was heated from 10 to 310 K, increasing the temperature by 10 K every 100 ps. Then, 2 ns simulations at 310 K were performed. Third, equilibration was performed in the NpT ensemble with a constant pressure of 1 atm controlled by using the Langevin Piston method and at constant temperature of 310 K regulated by Langevin dynamics with a damping factor of 1 ps^{-1} . During 5 ns equilibration, the restraints were exponentially decreased in 50 time windows (scaled from 1 to 0.0065). Further, the 120 ns production runs were performed without any restraints. Periodic boundary conditions and the Particle Mesh Ewald method with a grid spacing of 1 Å were used. The SHAKE algorithm and an integration time step of 2 fs were applied. For nonbonded interactions, a short-range cutoff of 12 Å was used.

In order to calculate the GaMD acceleration parameters, the original simulation experiments were followed by the GaMD simulation^[38,39] experiments with an additional 2 ns of MD simulation. After adding the boost potential, the simulation was continued for 30 ns to equilibrate the system. Subsequently, ten independent GaMD production runs were conducted for 100 ns each, starting with randomized initial atomic velocities. The GaMD simulations were performed in the dual-boost mode, in which the boost potential was applied to the dihedral and total potential energy terms. The threshold energy was set to the lower bound, that is, $E = V_{\text{max}}$. The upper limit of the boost potential standard deviation, σ_0 , was set to 10 kcal mol^{-1} for the dihedral and total potential energetic terms.

Acknowledgements

The authors thank Prof. Colin Kleanthous (Oxford University) for providing ColE3 toxin, Dr. Eli Shulman for performing the initial RNase tests by gel electrophoresis, and Dr. Moran Shalev for helping in the initial design and modeling experiments. This work was supported by research grants from the Israel Science Foundation founded by the Israel Academy of Sciences and Humanities (grant no. 1845/14 for T.B.); the Ministry of Science, Technology and Space, State of Israel (grant no. 2022675 for T.B.); the Interdisciplinary Centre for Mathematical and Computational Modelling University of Warsaw (grants G31-4, GA65-16, GA73-21 for J.T. and T.P.); and the National Science Centre, Poland (UMO-2017/26/M/NZ1/00827). J.T. acknowledges the Polish-U.S. Fulbright Commission. V.B. acknowledges financial support by the Ministry of Immigration Absorption and the Ministry of Science and Technology, Israel (Kamea Program).

Conflict of Interest

The authors declare no conflict of interest.

Keywords: aminoglycosides • antibiotics • bacterial ribosomes • catalytic antibiotics • RNA

- [1] B. Bozdogan, L. Ednie, K. Credito, K. Kosowska, P. C. Appelbaum, *Antimicrob. Agents Chemother.* **2004**, *48*, 4762–4765.
- [2] B. I. Eisenstein, *Expert Opin. Invest. Drugs* **2004**, *13*, 1159–1169.
- [3] V. Pokrovskaya, I. Nudelman, J. Kandasamy, T. Baasov, *Methods Enzymol.* **2010**, *478*, 437–462.
- [4] J. Suh, W. S. Chei, *Curr. Opin. Chem. Biol.* **2008**, *12*, 207–213.
- [5] Z. Yu, J. A. Cowan, *Chem. Eur. J.* **2017**, *23*, 14113–14127.
- [6] T. Niittymäki, H. Lonnberg, *Org. Biomol. Chem.* **2006**, *4*, 15–25.
- [7] T. Lönnerberg, K. M. Kero, *Org. Biomol. Chem.* **2012**, *10*, 569–574.
- [8] R. Salvio, R. Cacciapaglia, L. Mandolini, F. Sansone, A. Casnati, *RSC Adv.* **2014**, *4*, 34412–34416.
- [9] S. Magnet, J. S. Blanchard, *Chem. Rev.* **2005**, *105*, 477–498.
- [10] A. Sreedhara, A. Patwardhan, J. A. Cowan, *Chem. Commun.* **1999**, *2*, 1147–1148.
- [11] A. Patwardhan, J. A. Cowan, *Dalton Trans.* **2011**, *40*, 1795–1801.
- [12] W. Szczepanik, A. Krezel, M. Brzezowska, E. Dworniczek, M. Jezowska-Bojczuk, *Inorg. Chim. Acta* **2008**, *361*, 2659–2666.
- [13] W. Szczepanik, J. Ciesiolka, J. Wrzesiński, J. Skala, M. Jezowska-Bojczuk, *Dalton Trans.* **2003**, 1488–1494.
- [14] W. Szczepanik, E. Dworniczek, J. Ciesiolka, J. Wrzesiński, J. Skala, M. Jezowska-Bojczuk, *J. Inorg. Biochem.* **2003**, *94*, 355–364.
- [15] S. M. K. Takahashi, *Acad. Press. New York* **1982**, 435–468.
- [16] X. J. Yang, T. Gerczei, L. Glover, C. C. Correll, *Nat. Struct. Biol.* **2001**, *8*, 968–973.
- [17] P. B. Rupert, A. R. Ferre-D'Amare, *Nature* **2001**, *410*, 780–786.
- [18] C. L. Ng, K. Lang, N. A. G. Meenan, A. Sharma, A. C. Kelley, C. Kleanthous, V. Ramakrishnan, *Nat. Struct. Mol. Biol.* **2010**, *17*, 1241–1246.
- [19] B. François, R. J. M. Russell, J. B. Murray, F. Aboul-ela, B. Masquida, Q. Vicens, E. Westhof, *Nucleic Acids Res.* **2005**, *33*, 5677–5690.
- [20] C. L. Ng, K. Lang, N. A. G. Meenan, A. Sharma, *Nat. Struct. Mol. Biol.* **2010**, *17*, 1241–1246.
- [21] M. Komiyama, K. Yoshinari, *J. Org. Chem.* **1997**, *62*, 2155–2160.
- [22] K. Yoshinari, M. Komiyama, *Chem. Lett.* **1990**, *19*, 519–522.
- [23] R.-B. B. Yan, M. Yuan, Y. F. Wu, X. F. You, X.-S. S. Ye, *Bioorg. Med. Chem.* **2011**, *19*, 30–40.
- [24] K. C. Nicolaou, V. A. Adsool, C. R. H. Hale, *Org. Lett.* **2010**, *12*, 1552–1555.
- [25] N. S. Chindarkar, A. H. Franz, *ARKIVOC (Gainesville, FL, U.S.)* **2008**, 21.
- [26] R. Pathak, D. Perez-Fernandez, R. Nandurdikar, S. K. Kalapala, E. C. Bottger, A. Vasella, *Helv. Chim. Acta* **2008**, *91*, 1533–1552.
- [27] R. Pathak, E. C. C. Böttger, A. Vasella, *Helv. Chim. Acta* **2005**, *88*, 2967–2985.
- [28] E. D. Goddard-Borger, R. V. Stick, *Org. Lett.* **2007**, *9*, 3797–3800.
- [29] V. Pokrovskaya, V. Belakhov, M. Hainrichson, S. Yaron, T. Baasov, *J. Med. Chem.* **2009**, *52*, 2243–2254.
- [30] J. Kondo, M. Hainrichson, I. Nudelman, D. Shallom-Shezi, C. M. C. M. Barbieri, D. S. D. S. Pilch, E. Westhof, T. Baasov, *ChemBioChem* **2007**, *8*, 1700–1709.
- [31] M. T. G. Holden, E. J. Feil, J. A. Lindsay, S. J. Peacock, N. P. J. Day, M. C. Enright, T. J. Foster, C. E. Moore, L. Hurst, R. Atkin, et al., *Proc. Natl. Acad. Sci. USA* **2004**, *101*, 9786–9791.
- [32] G. Kaneti, H. Sarig, I. Marjeh, Z. Fadia, A. Mor, *FASEB J.* **2013**, *27*, 4834–4843.
- [33] J. I. Sekiguchi, T. Asagi, T. Miyoshi-Akiyama, T. Fujino, I. Kobayashi, K. Morita, Y. Kikuchi, T. Kuratsuji, T. Kirikae, *Antimicrob. Agents Chemother.* **2005**, *49*, 3734–3742.
- [34] M. Hainrichson, O. Yaniv, M. Cherniavsky, I. Nudelman, D. Shallom-Shezi, S. Yaron, T. Baasov, *Antimicrob. Agents Chemother.* **2007**, *51*, 774–776.
- [35] B. a. Maguire, L. M. Wondrack, L. G. Contillo, Z. Xu, *RNA* **2008**, *14*, 188–195.
- [36] P. Pfister, S. Hobbie, Q. Vicens, E. C. Böttger, E. Westhof, *ChemBioChem* **2003**, *4*, 1078–1088.
- [37] Q. Vicens, E. Westhof, *Chem. Biol.* **2002**, *9*, 747–755.
- [38] Y. Miao, V. A. Feher, J. A. McCammon, *J. Chem. Theory Comput.* **2015**, *11*, 3584–3595.
- [39] Y. T. Pang, Y. Miao, Y. Wang, J. A. McCammon, *J. Chem. Theory Comput.* **2017**, *13*, 9–19.
- [40] C. C. Correll, X. Yang, T. Gerczei, J. Beneken, M. J. Plantinga, *J. Synchrotron Radiat.* **2004**, *11*, 93–96.
- [41] M. J. Belousoff, B. Graham, L. Spiccia, Y. Tor, *Org. Biomol. Chem.* **2009**, *7*, 30–33.

- [42] R. J. Leatherbarrow, *GraFit 5*, Erithacus Software Ltd., Horley, U.K., **2001**.
- [43] NCCLS, National Committee for Clinical Laboratory Standards, Performance Standards for Antimicrobial Susceptibility Testing. Fifth Information Supplement: Approved Standard M100-S5, NCCLS, Villanova, PA, **1994**.
- [44] S. Carr, D. Walker, R. James, C. Kleanthous, A. M. Hemmings, *Structure* **2000**, *8*, 949–960.
- [45] J. C. Phillips, R. Braun, W. Wang, J. Gumbart, E. Tajkhorshid, E. Villa, C. Chipot, R. D. Skeel, L. Kalé, K. Schulten, *J. Comput. Chem.* **2005**, *26*, 1781–1802.

Manuscript received: September 13, 2018
 Revised manuscript received: November 20, 2018
 Accepted manuscript online: November 25, 2018
 Version of record online: December 21, 2018
